Vortex Configurations in High-T_c Superconducting Films[*]

Hans G. Kaper and Man Kam Kwong

Mathematics and Computer Science Division
Argonne National Laboratory
Argonne, IL 60439-4801

November 23, 1992

Abstract

This article addresses the Ginzburg-Landau (GL) model for high-temperature super-conductivity in thin films (two-dimensional periodic domains). A new gauge is defined to reduce the coupling between the equations for the nonzero components of the vector potential. The GL equations are written in a novel form by means of continuous link variables; this form is symmetric and has particular advantages for numerical analysis. The continuous GL model is approximated by a discrete model, which is shown to be second-order accurate. Two methods are used for the numerical solution of the discrete model—a modified Newton's method, in combination with a sweeping algorithm for the solution of the linear system, and a time-like integration method based on gradient flow. Numerical experiments demonstrate that the discrete GL model leads to asymmetric solutions in the plane; symmetry is recovered only in the limit as the mesh size goes to zero. The results of computational experiments to find the upper critical field and establish an empirical power law for vortex interactions are given.

AMS(MOS) subject classification. Primary 81J05. Secondary 82A25, 65N05, 35J60.

Key words and phrases. Ginzburg-Landau model, high-temperature super-conductivity, thin film, periodic domain, mixed state, vortex lattice, symmetry properties, gauge invariance, link variables.

1   Introduction

1.1   Statement of the Problem

In the Ginzburg-Landau (GL) theory [1], the physical state of a superconductor is described by two variables, the *order parameter* ψ and the *vector potential* $\mathbf{A}$. The quantity ψ is a complex scalar-valued function of position, which plays a role similar to the wave function in quantum mechanics; the square of its modulus, $|\psi|^2$, represents the local superelectron density. The quantity $\mathbf{A}$ is a real, three-dimensional, vector-valued function of position, which determines the electromagnetic variables; the induced magnetic field is $\mathbf{B} = \nabla \times \mathbf{A}$, and the superelectron current (the "supercurrent") density $\mathbf{j}_s$ is a multiple of $\nabla \times \mathbf{B} = \nabla \times \nabla \times \mathbf{A}$. A state of thermodynamic equilibrium corresponds to a global minimum of the Gibbs free energy. If Ω is the spatial domain occupied by the superconductor, then the expression for the Gibbs free energy (after a suitable nondimensionalization) is

$$\mathcal{G}(\psi, \mathbf{A}) = \int_\Omega \left(-|\psi|^2 + \tfrac{1}{2}|\psi|^4 + |(\nabla - i\mathbf{A})\psi|^2 + \kappa^2|\mathbf{B}|^2 - 2\kappa\mathbf{H} \cdot \mathbf{B} \right) d\mathbf{x}. \qquad \boxed{\text{(GFE)}}$$

Here, $\mathbf{H}$ is the applied magnetic field. In the normal (nonsuperconducting) state, $\psi = 0$ and the induced magnetic field $\mathbf{B}$ is proportional to $\mathbf{H}$; contributions to the Gibbs free energy from normal regions can be ignored for our purposes. The unit of length in (1.1) is the coherence length (the length scale for variations of ψ). The parameter κ is the *Ginzburg-Landau parameter*, which is the ratio of the London penetration depth (the length scale for variations of $\mathbf{B}$) and the coherence length.

As was first demonstrated analytically by Abrikosov [2], superconducting materials with $\kappa > 1/\sqrt{2}$ can sustain a spatially regular pattern of vortices, which are generated much like in fluid dynamics by the circular motion of superelectrons around normal cores. The supercurrent shields the superconducting region from the normal cores, thus preventing the magnetic flux lines from penetrating into the superconducting region.

Typical length scales in a flux line lattice are several orders of magnitude smaller than the size of a superconducting device, so a complete simulation of the latter is impossible. However, since the flux lines appear to align themselves in a regular spatial pattern, it is common practice to concentrate on the phenomena in the bulk of the medium and ignore boundary effects. We follow this practice and study the GL model on a periodic domain, choosing the boundary conditions on the unit cell in such a way that periodicity is imposed on *measurable* physical quantities, such as the current and the induced magnetic field.

In this article, we are concerned with thin-film superconductors in a uniform applied magnetic field normal to the plane of the film. This configuration gives rise to a two-dimensional problem on a periodic domain. The problem has been discussed by many authors, beginning with Abrikosov [2]. We mention in particular two recent articles by Du et al. [3] and [4], who discuss several mathematical aspects of the GL model and its numerical approximation by means of finite elements. The former of these two articles deals with GL models on bounded domains in two and three dimensions, the latter specifically

with GL models on two-dimensional periodic domains. The GL model in two-dimensional periodic domains has been the subject of several numerical investigations, most recently by means of optimization techniques; for example, see Doria et al. [5], Wang and Hu [6], and Garner et al. [7].

1.2   Summary of the Results

In this article we present at least six new results.

- We show that a discrete GL model leads to asymmetric solutions in the plane. Symmetry is recovered only in the limit as the mesh size goes to zero (Section 4.2).

- We define a new gauge in which the equations for the two nonzero components of the vector potential are only weakly coupled through the order parameter. The weak coupling leads to a significant reduction in the numerical computations (Section 2.2).

- We write the GL equations in a novel symmetric form by introducing a continuous analog of the link (or bond) variables commonly found in discrete GL models. The symmetric form has particular advantages from an analytical as well as numerical point of view (Section 2.3).

- Using the symmetric form of the GL equations, we prove that the discrete GL model, which is commonly derived by approximating first-order derivatives by means of forward differences, is in fact second-order accurate (Section 3.1).

- We determine the upper critical field through computational experiments (Section 4.3).

- We establish an empirical power law for vortex interactions (Section 4.4).

1.3   Outline of the Article

In Section 2, we discuss the continuous GL model. We introduce the canonical gauge and formulate the mathematical model in this gauge. In Section 3, we discuss the discrete GL model. We describe the approximation procedure and two numerical methods for the solution of the discrete model—a modified Newton's method, in combination with a sweeping algorithm for the solution of the linear system, and a time-like integration method based on gradient flow. In Section 4, we present the results of a series of numerical experiments. We show that the discrete GL model leads to asymmetric solutions in the plane; symmetry is recovered only in the limit as the mesh size goes to zero. We find the upper critical field and establish a heuristic power law for vortex interactions.

2 Ginzburg-Landau Model

2.1 Two-Dimensional Periodic Domain

In the present article we restrict ourselves to the case of a thin-film superconductor in a uniform applied field normal to the plane of the film. This problem is strictly two-dimensional; the order parameter varies in the plane of the film, and the vector potential has only two nonzero components, which lie in the plane of the film. Therefore, we identify the domain of the superconductor with $\mathbf{R}^2$, denoting the (Cartesian) coordinates by x and y and the x- and y-components of the vector potential by A_x and A_y, respectively. If H is the strength of the applied magnetic field, then $\mathbf{H} = (0, 0, H)$. The induced magnetic field is $\mathbf{B} = (0, 0, B)$, where $B = \partial_x A_y - \partial_y A_x$.

We are interested in solutions of the GL model that yield *measurable* quantities that are *periodic* in the plane. Given two arbitrary vectors $\mathbf{t}_1$ and $\mathbf{t}_2$ that span $\mathbf{R}^2$, we say that a function f is periodic with respect to the lattice determined by $\mathbf{t}_1$ and $\mathbf{t}_2$ if $f(\mathbf{x} + \mathbf{t}_k) = f(\mathbf{x})$ for $k = 1, 2$ and for all $\mathbf{x} = (x, y) \in \mathbf{R}^2$. The measurable quantities are the density of the superelectrons $|\psi|^2$, the induced magnetic field $\nabla \times \mathbf{A}$, and the supercurrent $\nabla \times \nabla \times \mathbf{A}$. These quantities are periodic if ψ and $\mathbf{A}$ (that is, A_x and A_y) satisfy the following conditions:

$$\psi(\mathbf{x} + \mathbf{t}_k) = \psi(\mathbf{x}) \exp(i g_{k\theta}(\mathbf{x})), \quad k = 1, 2, \qquad \boxed{\text{perp}} \qquad (2.1)$$

$$\mathbf{A}(\mathbf{x} + \mathbf{t}_k) = \mathbf{A}(\mathbf{x}) + (\nabla g_{k\theta})(\mathbf{x}), \quad k = 1, 2, \qquad \boxed{\text{perA}} \qquad (2.2)$$

for all $\mathbf{x} = (x, y) \in \mathbf{R}^2$, where

$$g_{k\theta}(\mathbf{x}) = C_k - \tfrac{1}{2}\overline{B}((1 + \theta)t_{ky}x - (1 - \theta)t_{kx}y), \quad k = 1, 2. \qquad \boxed{\text{gtheta}} (2.3)$$

Here, θ, C_1, and C_2 are arbitrary constants; cf. [4]. The constant $\overline{B}$ is the average (induced) magnetic field strength, which is determined by the number of vortices in a lattice cell. If this number is n, then

$$\overline{B} = \frac{2\pi n}{|\mathbf{t}_1 \times \mathbf{t}_2|}. \qquad \boxed{\text{Gamma}} \qquad (2.4)$$

Henceforth, we assume without loss of generality that $\mathbf{t}_1$ points into the right half of the (x, y)-plane and that $\mathbf{t}_2$ points in the direction of the positive y-axis. A convenient representation is

$$\mathbf{t}_1 = (\alpha L, \beta L)^T, \quad \mathbf{t}_2 = (0, L)^T, \qquad (2.5)$$

where $L > 0$, $\alpha > 0$, and β is a real number. We refer to α as the *aspect ratio* and β as the *lattice angle*.

Remark. It is common to reduce the complexity of the problem by assuming hexatic order and rotational symmetry in the plane. The only admissible values are then $\alpha = \sqrt{3}$ and $\beta = 1$. This reduction favors a particular class of solutions for no good reason. There is no *a priori* reason to assume hexatic order and rotational symmetry; if such symmetries

are present, they should follow from the model. In principle, one should keep α and β as free parameters in the model. We will do so in the following analysis and come back to this point in Section 4.

We now choose the constants θ, C_1, and C_2 in (2.3) to reduce the periodicity conditions (2.1) and (2.2) to their simplest form,

$$\theta = -1, \quad C_1 = 0, \quad C_2 = 0. \qquad \boxed{\text{th}} \qquad (2.6)$$

The choice of C_1 and C_2 is motivated by the fact that the phase of ψ will thus be the same at all vertices of the lattice. For $k = 1$, the conditions (2.1) and (2.2) yield a set of modified periodicity conditions,

$$\psi(x + \alpha L, y + \beta L) = \psi(x, y)e^{igy}, \qquad \boxed{\text{perxp}} \qquad (2.7)$$

$$A_x(x + \alpha L, y + \beta L) = A_x(x, y), \quad A_y(x + \alpha L, y + \beta L) = A_y(x, y) + g, \qquad \boxed{\text{perxA}} \qquad (2.8)$$

where

$$g = \alpha \overline{B} L = \frac{2\pi n}{L}. \qquad \boxed{\text{g}} \qquad (2.9)$$

For $k = 2$, the conditions (2.1) and (2.2) reduce to the usual periodicity conditions in the y-variable,

$$\psi(x, y + L) = \psi(x, y), \qquad \boxed{\text{peryp}} \qquad (2.10)$$

$$A_x(x, y + L) = A_x(x, y), \quad A_y(x, y + L) = A_y(x, y). \qquad \boxed{\text{peryA}} \quad (2.11)$$

These conditions must be satisfied at all points (x, y) in the plane.

Remark. There is no agreement in the literature on the choice of the constants θ, C_1, and C_2 in (2.3). For example, one finds the choice $\theta = 1$, $C_1 = 0$, and $C_2 = -\frac{1}{2}(\beta/\alpha)\overline{B}L^2$ in [8]; $\theta = 0$, $C_1 = 0$, and $C_2 = 0$ in [4] and [9]; the choice (2.6), with $\beta = 0$, is the same as in [5].

At this point, it is natural to identify the domain Ω with a unit cell of the lattice generated by $\mathbf{t}_1$ and $\mathbf{t}_2$—that is, to take for Ω the open parallelogram spanned by $\mathbf{t}_1$ and $\mathbf{t}_2$—and replicate the results obtained for Ω to the entire plane by repeated application of the periodicity conditions. This is indeed the approach taken by Du et al. in their analysis of the GL equations in [4]. However, because our model is fully periodic in the y-direction, we may as well identify Ω with the rectangle $[0, \alpha L] \times [0, L]$, so henceforth we take

$$\Omega = [0, \alpha L] \times [0, L]. \qquad \boxed{\text{O}} \qquad (2.12)$$

This identification explains the terms "aspect ratio" and "lattice angle" for α and β, respectively.

2.2 Canonical Gauge

The Gibbs free energy functional (1.1) is *gauge invariant*. That is,

$$\mathcal{G}(\psi, \mathbf{A}) = \mathcal{G}(\overline{\psi}, \overline{\mathbf{A}}), \qquad \boxed{\text{ginv}} \tag{2.13}$$

for any two pairs $(\psi, \mathbf{A})$ and $(\overline{\psi}, \overline{\mathbf{A}})$ that are related by an identity of the form

$$\overline{\psi} = \psi e^{i\chi}, \quad \overline{\mathbf{A}} = \mathbf{A} + \nabla\chi, \qquad \boxed{\text{gauge}} \tag{2.14}$$

where the *gauge* χ is a real-valued function of position. The pairs $(\psi, \mathbf{A})$ and $(\overline{\psi}, \overline{\mathbf{A}})$ give the same superelectron density, supercurrent, and magnetic field, so they can be considered as equivalent representations of the same state of the material. By varying the gauge, one obtains an entire class of equivalent representations. Choosing a gauge amounts to deciding on a canonical representative from a class of gauge-equivalent representations. This extra degree of freedom, which is inherent in the GL model, can be used to considerable advantage. By tailoring the gauge to the particular problem of interest, one can always single out the most appropriate canonical representative and study the problem in its simplest form.

Lemma 1 $\boxed{\text{L1}}$ *For any triple (ψ, A_x, A_y) satisfying the periodicity conditions (2.7)–(2.11) and any real number γ, there exists a gauge-equivalent triple $(\overline{\psi}, \overline{A}_x, \overline{A}_y)$ satisfying the same periodicity conditions, such that (i) $\arg \overline{\psi}(0,0) = 0$; (ii) $\overline{A}_x(x, \gamma x) = \overline{A}_x(0,0)$ for all x; and (iii) $\overline{A}_y(x, y) = \overline{A}_y(x, 0)$ for all (x, y).*

Proof. Take

$$\chi(x, y) = c + \int_{\gamma x}^{y} [a_y(x) - A_y(x, \eta)] \, d\eta$$
$$+ \int_0^x [a_x - A_x(\xi, \gamma\xi) + \gamma\{a_y(\xi) - A_y(\xi, \gamma\xi)\}] \, d\xi, \tag{2.15}$$

where

$$c = \begin{cases} -\arg \psi(0,0) & \text{if } \psi(0,0) \neq 0, \\ 0 & \text{if } \psi(0,0) = 0, \end{cases}$$

$$a_y(x) = \frac{1}{L} \int_0^L A_y(x, \eta) d\eta,$$

$$a_x = \frac{1}{\alpha L} \int_0^{\alpha L} [A_x(\xi, \gamma\xi) - \gamma\{a_y(\xi) - A_y(\xi, \gamma\xi)\}] \, d\xi,$$

and use the gauge transformation (2.14). ▮

We refer to the gauge defined in Lemma 1 as the *canonical gauge*. From now on, we always assume that the canonical gauge has been chosen and use (ψ, A_x, A_y) to denote the resulting canonical representative. Hence, ψ is real-valued at the origin, A_x is constant along the line $y = \gamma x$ for some real γ, and A_y is a function of x only. Normally, we take $\gamma = 0$, so A_x is constant along the lower egde of Ω.

Remark. Doria et al. [5] erroneously claimed that the gauge can be chosen so that A_x is *identically zero*. The error was pointed out by Wang and Hu [6]. While it is true that there exists a member in the equivalence class for which A_x is identically equal to zero, this member may not satisfy the periodicity conditions.

2.3   Ginzburg-Landau Equations

We now consider the Gibbs free energy and show how the canonical gauge simplifies the contributions from the magnetic field in (1.1).

First of all, the contribution from the applied magnetic field to the Gibbs free energy is constant and equal to $4\pi n\kappa H$. It can therefore be ignored for our purposes.

Second, because A_y is independent of y and A_x is periodic in y, the integral of the cross product $(\partial_x A_y)(\partial_y A_x)$ over Ω vanishes:

$$\int_\Omega (\partial_x A_y)(\partial_y A_x) \, dx\,dy = \int_0^{\alpha L} (\partial_x A_y) \int_0^L (\partial_y A_x) \, dy \, dx = 0. \qquad \boxed{\text{cross}} (2.16)$$

Hence, in the canonical gauge we have

$$\int_\Omega |\mathbf{B}|^2 \, d\mathbf{x} = \int_\Omega |\partial_x A_y - \partial_y A_x|^2 \, dx\,dy = \int_\Omega \left((\partial_y A_x)^2 + (\partial_x A_y)^2 \right) dx\,dy. \qquad \boxed{\text{kin}} (2.17)$$

Thus, the relevant expression for the Gibbs free energy in the canonical gauge is

$$\mathcal{G}(\psi, A_x, A_y) = \int_\Omega \left(-|\psi|^2 + \tfrac{1}{2}|\psi|^4 \right) dx\,dy$$

$$+ \int_\Omega \left(|(\partial_x - iA_x)\psi|^2 + |(\partial_y - iA_y)\psi|^2 + \kappa^2(\partial_y A_x)^2 + \kappa^2(\partial_x A_y)^2 \right) dx\,dy. \quad (2.\boxed{18})$$

The usual GL equations are obtained from (2.18) by minimizing $\mathcal{G}$ over the class of admissible triples (ψ, A_x, A_y). Here, admissibility is determined by the periodicity conditions (2.7), (2.8), (2.10), and (2.11), and by the constraint that A_x be constant along the line $y = \gamma x$ for some real γ. In the canonical gauge, the periodicity conditions reduce to

$$\psi(\alpha L, y + \beta L) = \psi(0, y)\mathrm{e}^{igy}, \quad A_x(\alpha L, y + \beta L) = A_x(0, y), \quad A_y(\alpha L) = A_y(0) + g, \quad (2.\boxed{\text{perx}})$$

for all $y \in [0, L]$, and

$$\psi(x, L) = \psi(x, 0), \quad A_x(x, L) = A_x(x, 0), \qquad \boxed{\text{pery}} \qquad (2.20)$$

for all $x \in [0, \alpha L]$. We recall that $g = 2\pi n/L$, where n is the number of vortices per unit cell. In (2.19), the argument $y + \beta L$ must be taken $\mathrm{mod}(L)$ to achieve a value in the interval $[0, L]$.

However, we prefer to introduce new variables before we take variations. These variables are the *link* or *bond variables*,

$$U_x(x, y) = \mathrm{e}^{i \int^x A_x(\xi, y) \, d\xi}, \quad U_y(x, y) = \mathrm{e}^{i \int^y A_y(x, \eta) \, d\eta}. \qquad (2.21)$$

7

(The specific values of the lower limits on the integrals are irrelevant.) The link variables are normally introduced only in the context of the discrete GL model to restore gauge invariance [10]. In the canonical gauge, $U_y(x, y) = e^{iA_y(x)y}$. Without changing its value, we write $\mathcal{G}$ in the form

$$\mathcal{G}(\psi, A_x, A_y) = \int_\Omega \left(-|\psi|^2 + \tfrac{1}{2}|\psi|^4 \right) dx\,dy$$
$$+ \int_\Omega \left(|\partial_x(U_x^*\psi)|^2 + \left|\partial_y(U_y^*\psi)\right|^2 + \kappa^2(\partial_y A_x)^2 + \kappa^2(\partial_x A_y)^2 \right) dx\,dy. \qquad \boxed{\text{G}}(2.22)$$

Minimizing this expression over all admissible triples (ψ, A_x, A_y) leads to a symmetric form of the GL equations, which has advantages from an analytical as well as numerical point of view. The GL equations are

$$U_x\partial_x^2(U_x^*\psi) + U_y\partial_y^2(U_y^*\psi) + \left(1 - |\psi|^2\right)\psi \;\; = \;\; 0 \quad \text{on } \Omega, \qquad \boxed{\text{glp}} \qquad (2.23)$$

$$\kappa^2\partial_y^2 A_x + \left(\text{Im}(\psi^*\partial_x\psi) - |\psi|^2 A_x\right) \;\; = \;\; 0 \quad \text{on } \Omega, \qquad \boxed{\text{glA}} \qquad (2.24)$$

$$\kappa^2 A_y'' + \frac{1}{L}\int_0^L \left(\text{Im}(\psi^*\partial_y\psi) - |\psi|^2 A_y\right) dy \;\; = \;\; 0 \quad \text{on } [0, \alpha L]. \qquad \boxed{\text{glB}}(2.25)$$

A superscript * denotes complex conjugation, a superscript ′ differentiation with respect to x. Note that (2.23) and (2.24) are partial differential equations, while (2.25) is an ordinary differential equation. The equations (2.24) and (2.25) are only weakly coupled, in the sense that the coupling is indirect through ψ. This is an immediate result of the choice of the canonical gauge.

Notice that α and β, which are free parameters, do not occur in the differential equations. However, they enter (nonlinearly) into the solution through the boundary conditions (2.19). Consequently, the correct procedure is to solve the boundary value problem for the triple (ψ, A_x, A_y) on Ω for given values of α and β, to compute the value of the free energy for each solution, and then to minimize the free energy with respect to α and β. Once α and β and the corresponding triple (ψ, A_x, A_y) are known on Ω, we extend the solution to the entire plane by replication.

2.4   Properties of the Solution

The following lemma shows that the superelectron density in the mixed state is less than the superelectron density in the ideal (i.e., Meissner) state. Its proof provides yet another illustration how gauge invariance can be used to find the simplest representation of a particular problem.

Lemma 2 $\boxed{\text{L2}}$ If (ψ, A_x, A_y) is a solution of the GL equations, then either $|\psi| < 1$ everywhere or $|\psi| = 1$ everywhere.

Proof. Suppose that $|\psi|$ has a maximum at some point P. This maximum is positive, so there must be a neighborhood $\mathcal{N}(P)$ of P where ψ does not vanish. Then we can choose the gauge χ such that ψ is real in $\mathcal{N}(P)$; we need only to take $\chi = -\arg\psi$ in $\mathcal{N}(P)$.

The equation (2.23) consists of a real and an imaginary part. Near P, the real part reads

$$\partial_x^2 \psi + \partial_y^2 \psi + (1 - \psi^2)\psi = 0. \tag{2.26}$$

Here, the sum of the first two terms is negative or at most zero at P, so it must be the case that $\psi \leq 1$ at P. If $\psi = 1$ at some point in the interior of $\mathcal{N}(P)$, then it follows from the maximum principle that $\psi = 1$ everywhere inside $\mathcal{N}(P)$. The proof is now completed by means of a compactness argument. $\blacksquare$

The gauge used in the proof of the lemma cannot be defined continuously in the neighborhood of a vortex point, where ψ vanishes, so the assumption that ψ is real holds at best locally. Another proof of Lemma 2 can be found in [4].

With $\psi = |\psi| \mathrm{e}^{i\phi}$, the expression for the supercurrent density is

$$\mathbf{j}_s = |\psi|^2 (\partial_x \phi - A_x, \partial_y \phi - A_y, 0)^T. \qquad \boxed{\text{js}} \tag{2.27}$$

Remark. It seems impossible to obtain the expression (2.27) directly from the functional (2.22) and the GL equations (2.23)–(2.25). In terms of A_x and A_y, we have $\mathbf{j}_s = \kappa^2 (-\partial_y^2 A_x, \partial_x \partial_y A_x - \partial_x^2 A_y, 0)^T$. From (2.24) we obtain the (pointwise) identity $-\kappa^2 \partial_y^2 A_x = |\psi|^2 (\partial_x \phi - A_x)$ and thereby the x-component of the supercurrent density given in (2.27). But the y-component cannot be obtained in this way; in fact, using the periodicity condition (2.20) for A_x, we find from (2.25) that

$$\int_0^L \kappa^2 (\partial_x \partial_y A_x - \partial_x^2 A_y)\, dy = \int_0^L |\psi|^2 (\partial_y \phi - A_y)\, dy, \tag{2.28}$$

so while it is true that the identity

$$\kappa^2 (\partial_x \partial_y A_x - \partial_x^2 A_y) = |\psi|^2 (\partial_y \phi - A_y) \qquad \boxed{\text{j}} \tag{2.29}$$

holds *in the mean* (that is, averaged over the interval $[0, L]$) for each $x \in [0, \alpha L]$, we cannot conclude that (2.29) is true *pointwise* (that is, for each (x, y) in Ω). On the other hand, (2.29) follows directly when we apply the variational method to (1.1). Since the canonical gauge does not affect the expression for the current density, it must be the case that (2.29) holds pointwise.

3 Discrete Ginzburg-Landau Model

3.1 Approximation Procedure

We next proceed to discretize the GL model for the purpose of computation. We take as our computational domain the rectangle Ω and use a uniform grid of $N_x \times N_y$ points, not counting the points on the top and right boundaries of the rectangle. The latter are

9

identified with the corresponding points on the bottom and left boundaries, respectively. The grid spacings in the x- and y-directions are h_x and h_y,

$$h_x = \alpha L/N_x, \quad h_y = L/N_y. \tag{3.1}$$

We define the matrix $\psi \in \mathbf{C}^{N_x \times N_y}$, whose elements are the values of the order parameter at the gridpoints,

$$\psi_{ij} = \psi(ih_x, jh_y), \quad i = 0, \ldots, N_x - 1, \; j = 0, \ldots, N_y - 1. \tag{3.2}$$

Next, we define the matrix $A_x \in \mathbf{R}^{N_x \times N_y}$ by taking the values of the x-component of the vector potential at the midpoints of the horizontal grid edges,

$$A_{x,ij} = A_x((i + \tfrac{1}{2})h_x, jh_y), \quad i = 0, \ldots, N_x - 1, \; j = 0, \ldots, N_y - 1. \tag{3.3}$$

Since the y-component A_y of the vector potential does not vary in the vertical direction, we define the vector $A_y \in \mathbf{R}^{N_x}$ by taking

$$A_{y,i} = A_y(ih_x), \quad i = 0, \ldots, N_x - 1. \tag{3.4}$$

The various evaluation points are indicated in Figure 1 (left). To obtain a discrete approximation to the free-energy functional (2.22), we partition the domain Ω in four different ways. Let

$$\Omega_{ij} = \{(x,y) \in \Omega : (i - \tfrac{1}{2})h_x < x < (i + \tfrac{1}{2})h_x, (j - \tfrac{1}{2})h_y < y < (j + \tfrac{1}{2})h_y\}, \tag{3.5}$$

$$\Omega_{ij}^{\rightarrow} = \{(x,y) \in \Omega : ih_x < x < (i + 1)h_x, (j - \tfrac{1}{2})h_y < y < (j + \tfrac{1}{2})h_y\}, \tag{3.6}$$

$$\Omega_{ij}^{\uparrow} = \{(x,y) \in \Omega : (i - \tfrac{1}{2})h_x < x < (i + \tfrac{1}{2})h_x, jh_y < y < (j + 1)h_y\}, \tag{3.7}$$

$$\Omega_{ij}^{\nearrow} = \{(x,y) \in \Omega : ih_x < x < (i + 1)h_x, jh_y < y < (j + 1)h_y\}, \tag{3.8}$$

wrapping around at the edges of Ω. The various domains are illustrated in Figure 1 (right).
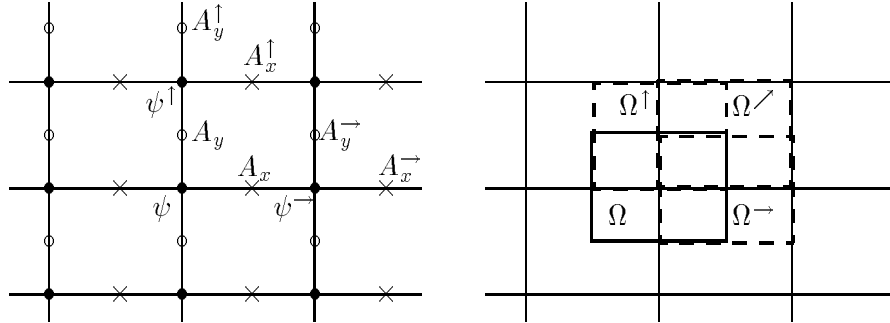

Figure 1: (Left) Evaluation points for ψ ($\bullet$), A_x ($\times$), and A_y ($\circ$). (Right) The domains Ω (solid frame), $\Omega^{\rightarrow}$, $\Omega^{\uparrow}$, and $\Omega^{\nearrow}$ (dashed frames).

Notice that the partitions are chosen in such a way that ψ_{ij} is the value of ψ at the center of Ω_{ij}, $A_{x,ij}$ the value of A_x at the center of $\Omega_{ij}^{\rightarrow}$, and $A_{y,i}$ the value of A_y at the center of $\Omega_{ij}^{\uparrow}$.

Without changing its value, we can write the free-energy functional in the form

$$
\mathcal{G}(\psi, A_x, A_y) = \sum_{ij} \int_{\Omega_{ij}} \left(-|\psi|^2 + \tfrac{1}{2}|\psi|^4 \right) \, dx\,dy
$$

$$
+ \sum_{ij} \int_{\Omega_{\overrightarrow{ij}}} \left(|\partial_x(U_x^*\psi)|^2 \right) \, dx\,dy + \sum_{ij} \int_{\Omega_{ij}^\uparrow} \left(\left| \partial_y(U_y^*\psi) \right|^2 \right) \, dx\,dy
$$

$$
+ \kappa^2 \sum_{ij} \int_{\Omega_{ij}^\diagup} (\partial_y A_x)^2 \, dx\,dy + \kappa^2 \sum_{ij} \int_{\Omega_{ij}^\diagup} (\partial_x A_y)^2 \, dx\,dy. \tag{3.9}
$$

We approximate each integral individually,

$$
\int_{\Omega_{ij}} \left(-|\psi|^2 + \tfrac{1}{2}|\psi|^4 \right) \, dx\,dy \approx \left(-|\psi_{ij}|^2 + \tfrac{1}{2}|\psi_{ij}|^4 \right) h_x h_y, \tag{3.10}
$$

$$
\int_{\Omega_{\overrightarrow{ij}}} |\partial_x(U_x^*\psi)|^2 \, dx\,dy \approx \left| \frac{U_x^*((i+1)h_x, jh_y)\psi_{i+1,j} - U_x^*(ih_x, jh_y)\psi_{i,j}}{h_x} \right|^2 h_x h_y
$$

$$
= \left| \frac{\psi_{i+1,j} - \exp\left(i \int_{ih_x}^{(i+1)h_x} A_x(x, jh_y)\, dx \right) \psi_{ij}}{h_x} \right|^2 h_x h_y
$$

$$
\approx \left| \frac{\psi_{i+1,j} - U_{x,ij}\psi_{ij}}{h_x} \right|^2 h_x h_y, \tag{3.11}
$$

$$
\int_{\Omega_{ij}^\uparrow} \left| \partial_y(U_y^*\psi) \right|^2 \, dx\,dy \approx \left| \frac{U_y^*(ih_x, (j+1)h_y)\psi_{i,j+1} - U_y^*(ih_x, jh_y)\psi_{i,j}}{h_y} \right|^2 h_x h_y
$$

$$
= \left| \frac{\psi_{i,j+1} - \exp\left(ih_y A_{y,i} \right) \psi_{ij}}{h_y} \right|^2 h_x h_y
$$

$$
= \left| \frac{\psi_{i,j+1} - U_{y,ij}\psi_{ij}}{h_y} \right|^2 h_x h_y, \tag{3.12}
$$

$$
\int_{\Omega_{ij}^\diagup} (\partial_y A_x)^2 \, dx\,dy \approx \left(\frac{A_{x,i,j+1} - A_{x,ij}}{h_y} \right)^2 h_x h_y, \tag{3.13}
$$

$$
\int_{\Omega_{ij}^\diagup} (\partial_x A_y)^2 \, dx\,dy \approx \left(\frac{A_{y,i+1,j} - A_{y,ij}}{h_x} \right)^2 h_x h_y. \tag{3.14}
$$

In the integrals over $\Omega_{\overrightarrow{ij}}$ and $\Omega_{ij}^\uparrow$, we have introduced the discrete link variables,

$$
U_{x,ij} = \mathrm{e}^{ih_x A_{x,ij}}, \quad U_{y,i} = \mathrm{e}^{ih_y A_{y,i}}, \tag{3.15}
$$

which are elements of a matrix $U_x \in \mathbf{R}^{N_x \times N_y}$ and a vector $U_y \in \mathbf{R}^{N_x}$, respectively. These are the same link variables that one commonly encounters in discrete GL models, where they are introduced in an *ad hoc* fashion to restore gauge invariance; cf. [10].

11

Summing over i and j, we thus obtain the following approximation to the free-energy functional (2.22):

$$
\begin{aligned}
\mathcal{G}_d(\psi, A_x, A_y) \;=\; & \sum_{\text{grid}} \left(-|\psi|^2 + \tfrac{1}{2}|\psi|^4 \right) h_x h_y \\
& + \sum_{\text{grid}} \left(\left| \frac{\psi^{\rightarrow} - U_x \psi}{h_x} \right|^2 + \left| \frac{\psi^{\uparrow} - U_y \psi}{h_y} \right|^2 + \kappa^2 \left| \frac{A_x^{\uparrow} - A_x}{h_y} \right|^2 \right. \\
& \left. + \kappa^2 \left| \frac{A_y^{\rightarrow} - A_y}{h_x} \right|^2 \right) h_x h_y. \qquad \boxed{\text{dG}} \tag{3.16}
\end{aligned}
$$

Here, the notation is obvious; the sums extend over all grid points, and neighboring points are indicated by arrows pointing in the appropriate direction. When it comes to boundary points, the notion of "neighbor" has to be interpreted in the usual way for a periodic domain, with an additional twist because of the modified periodicity conditions in the x variable. Because full periodicity is imposed in the y-direction, it suffices to simply wrap the rows around, identifying corresponding points on the lower and upper boundary of Ω and identifying values of the variables at these points. However, when wrapping the columns around, thus identifying corresponding points on the left and right boundaries, we must increase or decrease the phase of the order parameter by gy and the function A_y by g, as indicated by (2.19).

Lemma 3 $\boxed{\text{L3}}$ *The discrete functional (3.16) is a second-order approximation to the continuous functional (2.22),*

$$
\mathcal{G}(\psi, A_x, A_y) = \mathcal{G}_d(\psi, A_x, A_y) + O(h^2) \text{ as } h \to 0, \tag{3.17}
$$

where $h = \max\{h_x, h_y\}$.

Proof. The approximations to the integrals over the subdomains all involve evaluations of the integrands at the centers of the subdomains, and the derivatives at the centers are approximated by central differences. ∎

The functional (3.16) is invariant under a discrete gauge transformation,

$$
\overline{\psi} = \psi e^{i\chi}, \quad \overline{A_x} = A_x + \frac{\chi^{\rightarrow} - \chi}{h_x}, \quad \overline{A_y} = A_y + \frac{\chi^{\uparrow} - \chi}{h_y}. \qquad \boxed{\text{dgauge}} \tag{3.18}
$$

Here $\chi \in \mathbf{R}^{N_x \times N_y}$ is a matrix whose entries may be identified with the values of a continuous gauge function at the grid points, $\chi_{ij} = \chi(i h_x, j h_y)$.

3.2 Discrete Ginzburg-Landau Equations

The discrete Ginzburg-Landau equations are obtained either by minimizing $\mathcal{G}_d$ with respect to variations in (the real and imaginary part of) ψ_{ij}, $A_{x,ij}$, and $A_{y,i}$ or directly by evaluating

(2.23) at the grid points, (2.24) at the midpoints of the horizontal grid edges, and (2.25) at the midpoints of the vertical grid edges, and using central differences to approximate the derivatives. The equations are

$$\mathcal{F}[\psi] \ \equiv \ \mathcal{L}\psi + (1 - |\psi|^2)\psi = 0, \qquad \boxed{\text{Fp}} \tag{3.19}$$

$$\mathcal{F}_y[A_x] \ \equiv \ \kappa^2 \mathcal{L}_y A_x + \frac{\mathrm{Im}(\psi^* U_x^* \psi^{\rightarrow})}{h_x} = 0, \qquad \boxed{\text{FA}} \tag{3.20}$$

$$\mathcal{F}_x[A_y] \ \equiv \ \kappa^2 \mathcal{L}_x A_y + \frac{1}{N_y} \sum_{\text{column}} \frac{\mathrm{Im}(\psi^* U_y^* \psi^{\uparrow})}{h_y} = 0, \qquad \boxed{\text{FB}} \tag{3.21}$$

where $\mathcal{L}$ is a linear operator acting on $\mathbf{C}^{N_x \times N_y}$,

$$\mathcal{L}\psi \equiv \mathcal{L}(A_x, A_y)\psi = \frac{U_x^{\leftarrow} \psi^{\leftarrow} - 2\psi + U_x^* \psi^{\rightarrow}}{h_x^2} + \frac{U_y^{\downarrow} \psi^{\downarrow} - 2\psi + U_y^* \psi^{\uparrow}}{h_y^2}, \qquad \boxed{\text{L}} \tag{3.22}$$

$\mathcal{L}_y$ is a linear operator acting on $\mathbf{R}^{N_x \times N_y}$,

$$\mathcal{L}_y A_x = \frac{A_x^{\uparrow} - 2A_x + A_x^{\downarrow}}{h_y^2}, \qquad \boxed{\text{LA}} \tag{3.23}$$

and $\mathcal{L}_x$ is a linear operator acting on $\mathbf{R}^{N_x}$,

$$\mathcal{L}_x A_y = \frac{A_y^{\leftarrow} - 2A_y + A_y^{\rightarrow}}{h_x^2}. \qquad \boxed{\text{LB}} \tag{3.24}$$

When it comes to grid points on the boundary, the concept of "neighbor" in all these expressions has to be interpreted with proper account of the modified periodicity conditions, as explained after (3.16).

The following lemma gives some properties of the operators $\mathcal{L}$, $\mathcal{L}_x$, and $\mathcal{L}_y$.

Lemma 4 $\boxed{\text{L4}}$ *The operator $\mathcal{L}$ is negative-definite Hermitian. The operators $\mathcal{L}_x$ and $\mathcal{L}_y$ are negative semi-definite and symmetric.*

Proof. The operator $\mathcal{L}$ is the sum of two operators, $\mathcal{L}_1$ and $\mathcal{L}_2$, corresponding to the first and second term in (3.22), respectively, and each of these operators is in turn a direct sum of operators that act on one single row or column. The latter are Hermitian and negative semi-definite; more specifically, they are negative definite unless the elements of A_x or A_y involved are all zero. Since this cannot be the case for all the summands simultaneously, their sum must be negative definite.

The operators $\mathcal{L}_x$ and $\mathcal{L}_y$ are symmetric and negative semi-definite, but not negative definite; the constant vector is in the null space of each. ∎

At each grid point P, $\mathcal{L}\psi$ is a linear combination of the values of ψ at P and at its four neighbors (left, right, up, and down). The pattern is similar to the standard finite-difference discretization of the Laplacian, $\Delta\psi$, except that the coefficients depend on the

13

values of A_x and A_y at P and its neighbors. This obviously complicates matters, but as we shall demonstrate below, it is possible to design an efficient numerical scheme for the inversion of $\mathcal{L}$. The operators $\mathcal{L}_x$ and $\mathcal{L}_y$ are the standard finite-difference discretizations of the second-order ordinary differential operator in the x and y directions, respectively. Their inversion offers no specific difficulties.

It is a relatively simple matter to prove the analog of Lemma 2 for the discrete case—namely, that either $|\psi| < 1$ everywhere or $|\psi| = 1$ everywhere—for any solution (ψ, A_x, A_y) of the discrete Ginzburg-Landau equations. Again, one uses a gauge χ that renders ψ real at any point P where $|\psi|$ reaches a maximum and at each of the four neighbors of P and uses the real part of the equation (3.19). Note that, in this case, the gauge χ can be chosen such that ψ is real at *all* grid points, simply by taking $\chi = -\arg \psi$ if $\psi \neq 0$ and $\chi = 0$ otherwise. However, this gauge does not preserve the periodicity conditions.

3.3 Numerical Methods

The system of nonlinear equations (3.19), (3.20), (3.21) can be solved, for example, by Newton's method (or some modification thereof). Such an approach generally leads to a local minimum of the free-energy functional. We have implemented it, in combination with a sweeping method for solving the linear system of algebraic equations for the order parameter. We have also implemented an alternative method based on a parameterization of the system of equations by a time-like variable and a numerical integration of the resulting system along trajectories. This approach leads to a global minimum of the free-energy functional, as the functional decreases along trajectories. Both methods can be used for the computation of vortex lattice configurations, as we will show in the following section.

3.3.1 Newton's Method

The first method for solving the system of nonlinear equations (3.19), (3.20), (3.21) is a modified Newton's method.

A Newton's method leads to the following iterative scheme. Starting from a suitably chosen triple $(\psi^{(0)}, A_x^{(0)}, A_y^{(0)})$, one computes a sequence of triples $(\psi^{(n)}, A_x^{(n)}, A_y^{(n)})$, $n = 1, 2, \ldots$, as follows. At any step n, one first updates ψ by solving the equation

$$\left(\mathcal{L}^{(n-1)} + 1 - 2|\psi^{(n-1)}|^2\right)\left(\psi^{(n)} - \psi^{(n-1)}\right) - (\psi^{(n-1)})^2\left(\psi^{(n)*} - \psi^{(n-1)*}\right) = -\mathcal{F}[\psi^{(n-1)}]. \quad \boxed{\text{Np}}$$

$$(3.25)$$

Here, $\mathcal{L}^{(n-1)} = \mathcal{L}(A_x^{(n-1)}, A_y^{(n-1)})$. Having found $\psi^{(n)}$, one then updates A_x and A_y by solving the equations

$$\kappa^2 \mathcal{L}_y A_x^{(n)} - \text{Re}\left(\psi^{(n)*} U_x^{(n-1)*} \psi^{(n)\rightarrow}\right)(A_x^{(n)} - A_x^{(n-1)}) = -\mathcal{F}_y[A_x^{(n-1)}], \quad (3.26\boxed{\text{NA}}$$

$$\kappa^2 \mathcal{L}_x A_y^{(n)} - \frac{1}{N_y}\sum_{\text{column}} \text{Re}\left(\psi^{(n)*} U_y^{(n-1)*} \psi^{(n)\uparrow}\right)(A_y^{(n)} - A_y^{(n-1)}) = \mathcal{F}_x[A_y^{(n-1)}]. \quad (3.2\boxed{\text{NB}}$$

In a modified Newton's method, one takes the approximation

$$(\psi^{(n-1)})^2(\psi^{(n)*} - \psi^{(n-1)*}) \approx |\psi^{(n-1)}|^2(\psi^{(n)} - \psi^{(n-1)}) \qquad (3.28)$$

in (3.25) and the approximations

$$\mathrm{Re}(\psi^{(n)*}U_x^{(n-1)*}\psi^{(n)\rightarrow}) \approx |\psi^{(n)}|^2, \quad \mathrm{Re}(\psi^{(n)*}U_y^{(n-1)*}\psi^{(n)\uparrow}) \approx |\psi^{(n)}|^2, \qquad (3.29)$$

in (3.26) and (3.27), respectively. Thus, the equations reduce to

$$\left(\mathcal{L}^{(n-1)} + 1 - 3|\psi^{(n-1)}|^2\right)\left(\psi^{(n)} - \psi^{(n-1)}\right) = -\mathcal{F}[\psi^{(n-1)}], \qquad \boxed{\text{MNp}} \quad (3.30)$$

$$\kappa^2\mathcal{L}_y A_x^{(n)} - |\psi^{(n)}|^2(A_x^{(n)} - A_x^{(n-1)}) = -\mathcal{F}_y[A_x^{(n-1)}], \qquad \boxed{\text{MNA}} \quad (3.31)$$

$$\kappa^2\mathcal{L}_x A_y^{(n)} - \frac{1}{N_y}\sum_{\text{column}}|\psi^{(n)}|^2(A_y^{(n)} - A_y^{(n-1)}) = -\mathcal{F}_x[A_y^{(n-1)}]. \qquad \boxed{\text{MNB}} \quad (3.32)$$

There are still potential difficulties with this modified Newton's method. As we have seen (Lemma 4), the operator $\mathcal{L}$ is negative-definite Hermitian, so its dominant eigenvalue (λ_1) is negative. As long as $1 - 3|\psi^{(n)}|^2$ is less than $|\lambda_1|$, the operator in the left member of (3.30) is also negative-definite Hermitian, so (3.30) can be solved for the increment $\psi^{(n)} - \psi^{(n-1)}$, but this condition may not always be satisfied. In fact, we have found that λ_1 approaches 0 as the density of the vortices in Ω (i.e., the relative volume occupied by the vortices in Ω) decreases, in which case it becomes increasingly likely that $1 - 3|\psi|^2$ will exceed $|\lambda_1|$ and the modified Newton's method will fail to converge. For this reason, we have used a further modification, introducing a "damping factor" $\delta^{(n-1)}$ and replacing (3.30) by the general equation

$$(\mathcal{L}^{(n-1)} - \delta^{(n-1)})(\psi^{(n)} - \psi^{(n-1)}) = -\mathcal{F}[\psi^{(n-1)}]. \qquad \boxed{\text{dNp}} \quad (3.33)$$

We take $\delta^{(n-1)} = 1 - 3|\psi^{(n-1)}|^2$ or increase the value of $\delta^{(n-1)}$ as necessary to ensure that (3.30) is solvable. Similarly, we make use of damping factors in (3.31) and (3.32),

$$(\kappa^2\mathcal{L}_y - \delta_y^{(n-1)})(A_x^{(n)} - A_x^{(n-1)}) = -\mathcal{F}_y[A_x^{(n-1)}], \qquad \boxed{\text{dNA}} \quad (3.34)$$

$$(\kappa^2\mathcal{L}_x - \delta_x^{(n-1)})(A_y^{(n)} - A_y^{(n-1)}) = -\mathcal{F}_x[A_y^{(n-1)}], \qquad \boxed{\text{dNB}} \quad (3.35)$$

where $\delta_y^{(n-1)} = |\psi^{(n)}|^2$ and $\delta_x^{(n-1)} = (1/N_y)\sum_{\text{column}}|\psi^{(n)}|^2$, or we may take $\delta_y^{(n-1)}$ and $\delta_x^{(n-1)}$ equal to some positive constants for convenience.

The resulting sequence of triples $\{(\psi^{(n)}, A_x^{(n)}, A_y^{(n)})\}$ converges to a solution (ψ, A_x, A_y) of (3.19), (3.20), (3.21); in general, the rate of convergence will be affected by the choice of the damping factors in (3.33), (3.34), and (3.35).

We note that it may be computationally convenient to ignore the gauge choice (ii) of Lemma 1—that is, that A_x is constant along the line $y = \gamma x$ for some real γ—during most of the iterative process. The resulting iterates $A_x^{(n)}$ may vary nonsmoothly, but the canonical gauge transformation can be applied at the end of the entire computation or whenever needed to smooth out the irregularities.

15

3.3.2 Sweeping Algorithm

The system of equations (3.33) is usually solved as a matrix equation for the vector (of length $N_x \times N_y$) of unknowns ψ_{ij}. The coefficient matrix is sparse, so the solution can be accomplished by means of special sparse-matrix techniques of numerical linear algebra. This approach has been applied with success, for example by Jones and Plassmann [11].

We have applied an alternative approach, based on the *sweeping algorithm* described in [12]. The method is similar to the shooting method for the numerical solution of two-point boundary value problems for second-order differential equations.

In the sweeping algorithm, the system of equations (3.33) is viewed as a nonhomogeneous *stencil equation* for the unknown matrix ψ (of order $N_x \times N_y$),

$$S[\psi] \equiv C\psi + L\psi^{\leftarrow} + R\psi^{\rightarrow} + U\psi^{\uparrow} + D\psi^{\downarrow} = b. \qquad \boxed{\text{system}} \qquad (3.36)$$

Here, C, L, R, U, and D are given matrices of order $N_x \times N_y$, and b is a given matrix (also of order $N_x \times N_y$). (As usual, we suppress the column and row indices; for example, $C\psi \equiv (C\psi)_{ij} = C_{ij}\psi_{ij}$.) The stencil equation is governed by a five-point stencil, which connects each element to its four neighbors (left, right, up, and down). The stencil varies from one element to the next, but otherwise it is similar to that of the Laplacian on a rectangular mesh. (In the case of the Laplacian, the stencil is constant: $C = -4$, $L = R = U = D = 1$.)

In the present case, none of the elements of L and R vanish, so we can solve (3.36) for $\psi^{\rightarrow}$ or $\psi^{\leftarrow}$,

$$\psi^{\rightarrow} = R^{-1}\left(b - \left[C\psi + L\psi^{\leftarrow} + U\psi^{\uparrow} + D\psi^{\downarrow}\right]\right), \qquad \boxed{\text{right}} \qquad (3.37)$$

$$\psi^{\leftarrow} = L^{-1}\left(b - \left[C\psi + R\psi^{\leftarrow} + U\psi^{\uparrow} + D\psi^{\downarrow}\right]\right). \qquad \boxed{\text{left}} \qquad (3.38)$$

These two expressions enable us to compute the columns of the matrix ψ by sweeping to the right with (3.37) or to the left with (3.38), starting with any two adjacent columns of ψ.

The simplest one-dimensional sweeping algorithm goes as follows. We start by constructing a *trial solution* $\overline{\psi}$ of (3.36), letting the first two columns of ψ be identically zero and using (3.37) to compute the remaining $N_x - 2$ columns. The discrepancy between the solution ψ of (3.36) and the trial solution is measured by the error (column vector of length $2N_y$)

$$e = (b_{ij} - S[\overline{\psi}]_{ij})^t, \quad i = 0, \dots, N_y - 1, \quad j = N_x - 2, N_x - 1. \qquad (3.39)$$

Next, we construct $2N_y$ matrices y that all satisfy the homogeneous equation $S[y] = 0$. Starting from the first two columns, taking all elements but one in these two columns equal to 0 and the one nonzero element equal to 1, and putting this nonzero element successively in each of the $2N_y$ locations in these two columns, we generate the matrices y by applying the sweeping operation

$$y^{\rightarrow} = -R^{-1}\left(Cy + Ly^{\leftarrow} + Uy^{\uparrow} + Dy^{\downarrow}\right) \qquad \boxed{\text{hright}} \qquad (3.40)$$

from left to right. From each matrix y thus generated we take the last two columns to form a vector of length $2N_y$, $(-S[y]_{ij})^t$, $i = 0, \ldots, N_y - 1$, $j = N_x - 2, N_x - 1$, which we juxtapose to obtain a *rectifying matrix* $\mathcal{R}$. Thus, the columns of $\mathcal{R}$ represent the change in the error vector e if we modify the appropriate element in the initial columns of $\overline{\psi}$ by 1. Hence, to make e vanish, we must modify the initial columns of $\overline{\psi}$ by $\mathcal{R}^{-1}e$. The vector $-\mathcal{R}^{-1}e$ gives therefore the first two columns of the correct solution ψ of (3.36). The full matrix ψ is then found by one more sweep to the right. The sweeping algorithm thus requires the inversion of only one matrix of order $2N_y$; it is essentially a direct (as opposed to an iterative) method for inverting the stencil.

A bidirectional sweeping algorithm can be devised by choosing the initial columns in the center of the matrix ψ. The two sweeps can be performed in parallel.

One difficulty with the sweeping algorithm is that $\psi^{\rightarrow}$ and $\psi^{\leftarrow}$ can grow quite rapidly; the algorithm thus becomes prone to rounding errors. Furthermore, the rectifying matrix $\mathcal{R}$ becomes more ill-conditioned as N_x gets large. We have used two modifications to overcome these difficulties; cf. [12]. A *multistage sweeping algorithm* divides the columns into several smaller sweeping ranges. A rectifying matrix is computed for each range; the global rectifying matrix is then constructed either explicitly or implicitly from these local rectifying matrices. The algorithm is still a direct method for inverting the stencil. A *partial sweeping algorithm* divides ψ into subdomains, over each of which the stencil is solved under the assumption that the value of ψ is fixed outside the subdomain. The substencil is thus solved independently over each subdomain, and the algorithm parallelizes naturally. If the subdomains are small enough, the instability of the sweeping algorithm is no longer a problem. However, errors are introduced near the boundaries of the subdomains, since there is no communication across subdomain boundaries. If the matrix is negative definite, the iterative application of the partial sweeping algorithm gives a sequence that converges to the exact solution. In our experiments we have observed that the rate of convergence can be improved significantly if one decomposes the matrix ψ in two alternate ways, so that the subdomain boundaries of one decomposition fall into the interior of the subdomains of the other decomposition.

3.3.3   Integration Method

In some instances, we have observed that the modified Newton's method outlined in the preceding section does not converge to a global minimum of the free-energy functional but gets stuck at a local minimum. In such cases, which admittedly may be hard to recognize, it is useful to have an alternative method that will surely lead to the global minimum. For this purpose we use an integration method, where we introduce a time-like variable t and integrate the gradient flow,

$$\partial_t \psi = \mathcal{F}[\psi], \quad \partial_t A_x = \mathcal{F}_y[A_x], \quad \partial_t A_y = \mathcal{F}_x[A_y], \qquad \boxed{t} \qquad (3.41)$$

until the solution equilibrates. Although t is introduced purely for numerical reasons, the system of equations (3.41) may reflect, at least qualitatively, the time evolution of a super-conducting medium near T_c from a given initial state; see, for example, [13].

So far, all solution techniques for the time-dependent system use the method of relaxation, albeit the simple forward Euler method for parabolic equations. The difficulty is the severe limitation on the time step, $\Delta t < h_x h_y / 4$, needed to ensure convergence. We approximate the exponential functions generated by the operators $\mathcal{L}$, $\mathcal{L}_x$, and $\mathcal{L}_y$ (method of lines). Considerations based on the use of the spectral decomposition show that, when we use a sufficiently large time step, we retain the portion of the function that corresponds to the smallest eigenvalue of each of these operators.

4   Computational Experiments

4.1   Sample Configurations

We begin by providing a few sample configurations for different values of the input parameters. They were computed for unit cells $\Omega = [0, L\sqrt{3}] \times [0, L]$ on grids with equal numbers of mesh points in the x- and y-directions, $N_x = N_y = N$. In these computations, we did not minimize over the parameters α and β, but fixed $\alpha = \sqrt{3}$ and $\beta = 1$. Thus we imposed the constraint that the vortex configuration be hexagonal and rotationally symmetric in the plane. (Experiments with variable aspect ratios are reported in the next section.) The constraint (ii) of Lemma 1—that A_x be constant along the line $y = \gamma x$ for some real γ—was implemented with $\gamma = 0$, so A_x is constant along the lower (and upper) edge of the unit cell. Various (small, medium, and large) values of the Ginzburg-Landau parameter were considered, but the sample configurations presented here are all for $\kappa = 5$. The remaining parameter is the number of vortices per unit cell, n. All computations were done in double precision with Matlab 4.0 Beta 3. This programming environment enabled us to maintain flexibility and make changes without much effort.

Figure 2 shows a configuration with two vortices per unit cell. In the left part of the figure, we have plotted contour lines for the superelectron density $|\psi|^2$ ($|\psi|^2 < 0.25$ everywhere); each traversal of a contour yields a change of the phase of ψ by 2π. In the right part of the figure, we have plotted contour lines for the induced magnetic field B.

In Figure 3, we again have two vortices per unit cell, but the unit cell has four times the size of the unit cell in Figure 2. Consequently, the average induced magnetic field (right part of the figure) is reduced by a factor of four, according to (2.4), and the free energy is much smaller than in the case of Figure 2. Also, we are closer to the lower critical field H_{c1}, $|\psi|^2$ (left part of the figure) is larger on average than in Figure 2 (but still less than 1 everywhere), and the size of the vortices is much smaller.

Figure 4 demonstrates that the numerical method remains effective when the number of vortices per unit cell increases. The figure also illustrates the effect of the grid size. The configuration of Figure 4 is similar to that of Figure 2. The unit cell of Figure 4 is eight times that of Figure 2, but the number of vortices per unit cell is eight times larger, so the average magnetic field is the same in both cases, as is confirmed in the right part of the figure. The solution of Figure 4 could be obtained by replicating that of Figure 2. However,
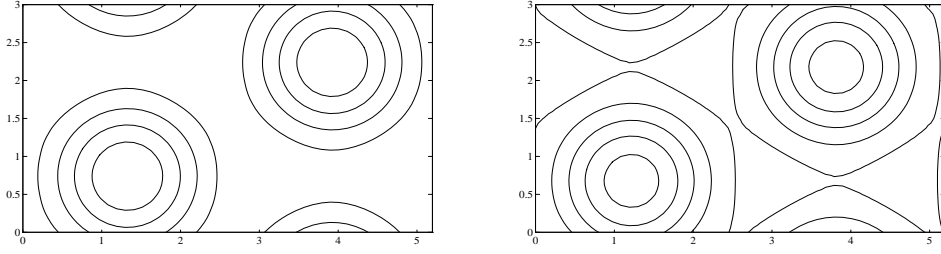
Figure 2: Sample configuration; $\kappa = 5$, $n = 2$, $L = 3$, $N = 24$. Free energy $\mathcal{G} = 16.2295\,4232$. (Left) Vortex configuration; contour lines for $|\psi|^2 = 0.05, 0.1, 0.15, 0.2$. (Right) Magnetic field; contour lines for $B = 0.804, 0.805, 0.806, 0.807, 0.808, 0.809$.
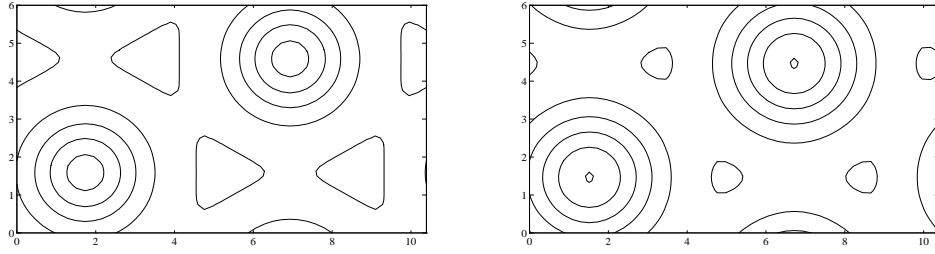

Figure 3: Sample configuration; $\kappa = 5$, $n = 2$, $L = 6$, $N = 24$. Free energy $\mathcal{G} = 0.7304\,0904$. (Left) Vortex configuration; contour lines for $|\psi|^2 = 0.1, 0.3, 0.5, 0.7, 0.9$. (Right) Magnetic field; contour lines for $B = 0.195, 0.200, 0.205, 0.210, 0.215$.

the solution of Figure 4 was computed on a 36×36 grid and that of Figure 2 on a 24×24 grid. The effect of the finer grid size is not visible in the contour lines, but it shows up in the value of the free energy: the average value of the free energy for a two-vortex cell that is of the same size as the unit cell of Figure 2 is slightly less than the free energy per unit cell in Figure 2.

4.2   Aspect Ratio and Symmetry

As we emphasized in Section 2, there is no *a priori* reason to assume hexatic order and rotational symmetry in the plane. If such symmetries exist, they should follow from the model. However, the assumptions are commonly made (as we did in the preceding section) to reduce the amount of computation. But by doing so, one restricts the class of admissible triples (ψ, A_x, A_y) over which one minimizes the free-energy functional. The problem is
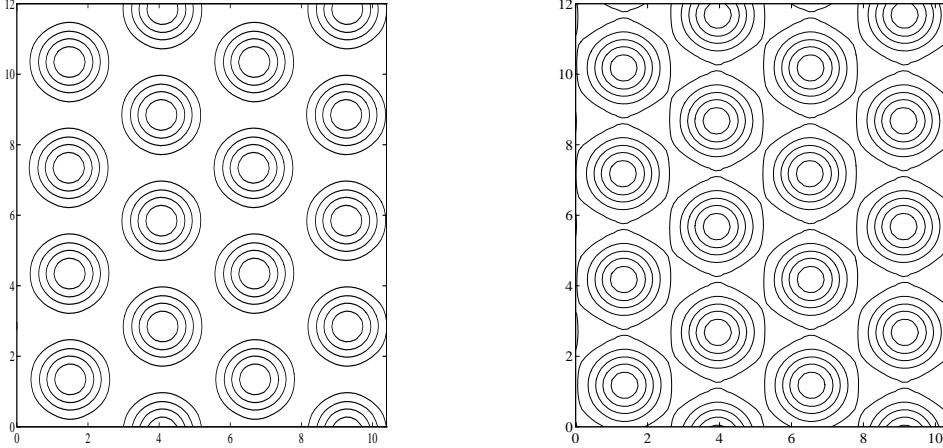
Figure 4: Sample configuration; $\kappa = 5$, $n = 16$, $L = 6$, $N = 36$. Average free energy per two-vortex cell $\mathcal{G} = 16.2286\ 1710$. (Left) Vortex configuration; contour lines for $|\psi|^2 = 0.05, 0.1, 0.15, 0.2$. (Right) Magnetic field; contour lines for $B = 0.804, 0.805, 0.806, 0.807, 0.808, 0.809$.

avoided only if one leaves the aspect ratio α and the lattice angle β free and performs an additional minimization with respect to these variables.

We designed a series of experiments to analyze, in particular, the effect of α. In these experiments we took a two-vortex cell with $\beta = 1$ and varied L and α, while keeping the area of the unit cell constant, $\alpha L^2 = 9\sqrt{3}$. Thus, if $\alpha = \sqrt{3}$, then $L = 3$ and we recover the configuration of Figure 2, which is hexagonal and rotationally symmetric. As in the preceding section, we took a grid with the same number of grid points in the x- and y-directions, $N_x = N_y = N$. Figure 5 gives a graph of the quantity $\mathcal{G} - 16.2295\ 4232$ associated with the minimum-energy configuration as a function of α. The smallest value of the minimum free energy occurs at $\alpha_{\mathrm{opt}} = 1.7818\ 8311$, which is greater than $\sqrt{3} = 1.7320\ 5081$. Hence, the computed vortex configuration is asymmetric.

The optimal aspect ratio α_{opt}, at which the computed free energy is minimal, varies with the grid, as can be seen from Table 1.

Table 1. Variation of the optimal aspect ratio with the number of grid points

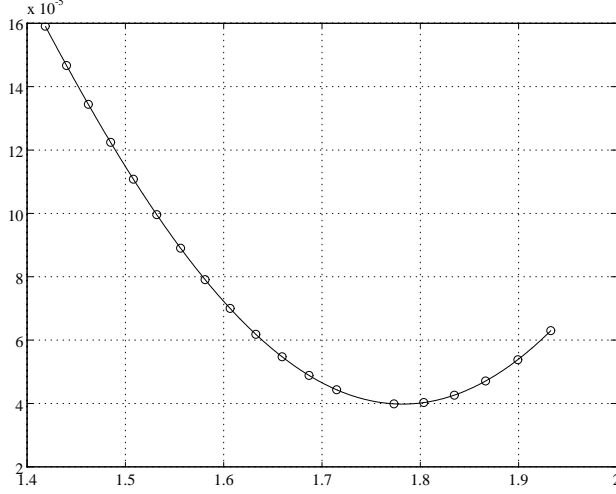| N	α_{opt}	N	α_{opt}
14	1.8780 0903	24	1.7818 8311
16	1.8438 4800	26	1.7745 4061
18	1.8204 4045	28	1.7687 0494
20	1.8037 1459	30	1.7639 9548
22	1.7913 2357		

Figure 5: Effect of the aspect ratio on the minimum free energy. The vertical coordinate is the quantity $\mathcal{G} - 16.2295\ 4232$ for the minimum-energy configuration, the horizontal coordinate is the aspect ratio α. Parameter values: $\kappa = 5$, $n = 2$, $N = 24$; $\alpha L^2 = 9\sqrt{3}$.

The data of Table 1 are plotted in Figure 6 (open circles). A second-degree extrapolation of the data in Table 1 gives $\lim_{N\to\infty} \alpha_{\mathrm{opt}} \approx 1.7320\ 71$, which is close to $\sqrt{3} = 1.7320\ 51$. Hence, it is fair to say that these experiments indicate that symmetry is recovered in the limit as the mesh size goes to zero.

4.3   Upper Critical Field

When a perfectly superconducting sample is subjected to an applied magnetic field of increasing strength, the superelectron density $|\psi|^2$ decreases until the sample enters the mixed state. The transition occurs at the lower critical field H_{c1}, when ψ first vanishes and one or more vortices begin to form. As the field strength increases further, the superelectron density decreases further until $\max\{|\psi(x,y)| : (x,y) \in \Omega\} = 0$. At that point, all superconductivity disappears and the sample enters the normal (i.e., nonsuperconducting) state. This transition occurs at the upper critical field H_{c2}. Computationally, one can simulate this physical experiment by decreasing the size of the unit cell, while keeping the number of vortices per unit cell fixed. The procedure is based on the discrete virial theorem of Doria et al. [14]; in our system of units, the virial theorem is

$$\kappa^2 \overline{B} H = \tfrac{1}{2}(\mathcal{G}_{\mathrm{kin}} + 2\mathcal{G}_{\mathrm{field}}), \qquad \boxed{\text{virial}} \tag{4.1}$$

where $\mathcal{G}_{\mathrm{kin}}$ and $\mathcal{G}_{\mathrm{field}}$ are the kinetic and field energy per unit area,

$$\mathcal{G}_{\mathrm{kin}} = \frac{1}{|\Omega|} \int_\Omega \left(|\partial_x(U_x^* \psi)|^2 + |\partial_y(U_y^* \psi)|^2 \right) \, dx\,dy, \qquad \boxed{\text{Ekin}} \tag{4.2}$$
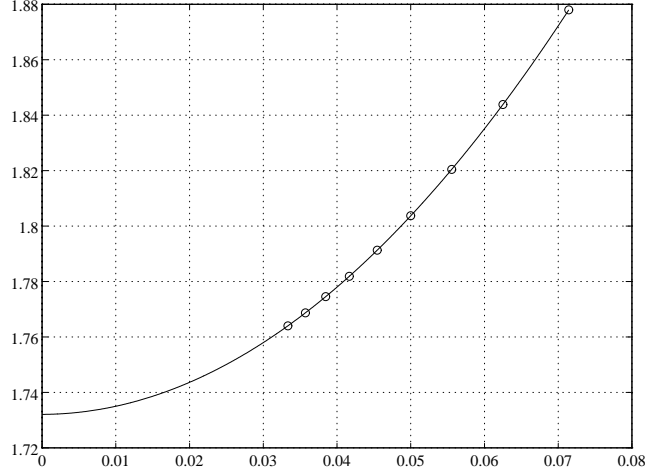
21

Figure 6: Variation of the optimal aspect ratio with the mesh size. The vertical coordinate is the optimal aspect ratio, the horizontal coordinate the reciprocal of the number of mesh points. The open circles represent computed values; the solid curve is a second-degree polynomial fit.

$$\mathcal{G}_{\text{field}} = \frac{1}{|\Omega|} \int_\Omega \left(\kappa^2 (\partial_y A_x)^2 + \kappa^2 (\partial_x A_y)^2 \right) \, dx \, dy. \qquad \boxed{\text{Efield}} \qquad (4.3)$$

We recall that $\overline{B}$, the average induced magnetic field, is related to the size of the domain and the number of vortices in the unit cell by (2.4). By decreasing L, while keeping n fixed, we increase the average induced magnetic field $\overline{B}$. Having found the solution (ψ, A_x, A_y), we compute the kinetic and field energy according to (4.2) and (4.3). Then the applied magnetic field H follows from (4.1).

Doria et al. used this procedure to compute the lower critical field H_{c1} in [5]. Here we demonstrate that the same procedure can be used to compute the upper critical field H_{c2}. In Figure 7, we present the result of such an experiment. The data are for a two-vortex cell, with $\alpha = \sqrt{3}$ and $\beta = 1$. The maximum value of the superelectron density is plotted against the external magnetic field. The density is zero when the external field H reaches the value $H_{c2} = 1.0031\ 6868$; at this point, $L = 2.68929$. The value of H_{c2} is close to 1, which is its value in the system of units adopted in this investigation.

4.4   Empirical Power Law

In a final experiment, we constructed a very simple model for vortex interactions. Assuming a hexagonal lattice and rotational symmetry in the plane, where d is the distance between a vortex and its nearest neighbor, we investigated the quality of an empirical power-law
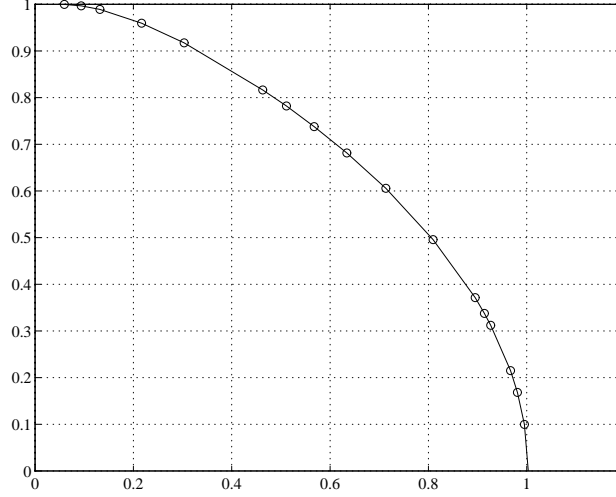
22

Figure 7: Calculation of the upper critical field H_{c2}. Graph of $\max |\psi|^2$ against the external field H for a sample with $\kappa = 5$.

interaction,

$$\mathcal{G} = a + bd^{-\gamma}, \qquad \boxed{\text{power}} \tag{4.4}$$

where a, b, and γ are constants, to be determined from the experiments. The graph plotting the free energy against d is shown in Figure 8. To test the suitability of such a power law, we used a portion of our data (marked by open circles in Figure 8) to determine the constants by means of a least-squares fit,

$$a = -0.2612\ 9173, \quad b = 1274.8, \quad \gamma = 3.9574. \tag{4.5}$$

We subsequently used these constants to plot the curve in Figure 8. The curve is seen to give an excellent fit to the remaining data (marked by crosses in Figure 8).
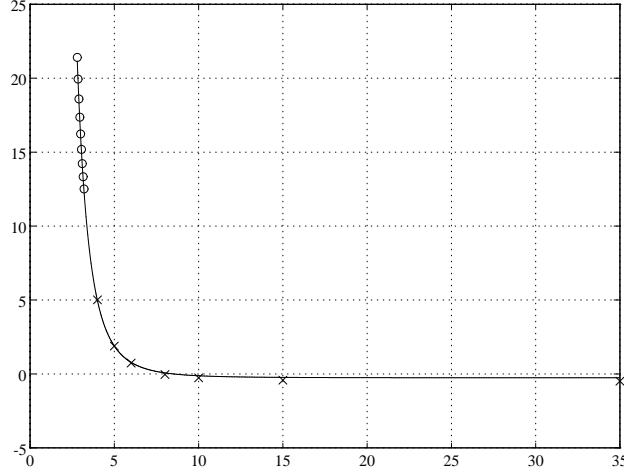
Figure 8: Empirical power law for vortex interaction. The graphc plots the free energy against the distance between neighboring vortices in a regular hexatic lattice.

References

[1] V. L. Ginzburg and L. D. Landau, "On the theory of superconductivity," *Zh. Eksperim. i Teor. Fiz.* **20** (1950), 1064–1082. [English translation in: D. ter Haar, *L. D. Landau, Men of Physics*, Vol. I. Pergamon Press, Oxford (1965), 138–167.]

[2] Abrikosov, A., "On the magnetic properties of superconductors of the second type," *Zh. Eksperim. i Teor. Fiz.* **32** (1957), 1442–1452. [English translation: *Soviet Phys. – JETP* **5** (1957), 1174–1182.]

[3] Q. Du, M. D. Gunzburger, and J. S. Peterson, "Analysis and approximation of the Ginzburg-Landau model of superconductivity," *SIAM Review* **34** (1992), 54–81.

[4] Q. Du, M. D. Gunzburger, and J. S. Peterson, "Modeling and analysis of a periodic Ginzburg-Landau model for type-II superconductors," preprint (1992).

[5] M. M. Doria, J. E. Gubernatis, and D. Rainer, "Solving the Ginzburg-Landau equations by simulated annealing," *Phys. Rev. B* **41** (1990), 6335–6340.

[6] Z. D. Wang, and C. R. Hu, "A numerical relaxation approach for solving the general Ginzburg-Landau equations for type-II superconductors," preprint (1991).

[7] J. Garner, M. Spanbauer, R. Benedek, K. Strandburg, S. Wright, and P. Plassmann, "Critical fields of Josephson-coupled superconducting multilayers," *Phys. Rev. B* **45** (1992) 7973–7983

[8] G. Eilenberger. "Zu Abrikosovs Theorie der periodischen Lösungen der GL-Gleichungen für Supraleiter 2. Art," *Zeitschrift f. Physik* **180** (1964), 32–42.

[9] F. Odeh, "Existence and bifurcation theorems for the Ginzburg-Landau equations," *J. Math. Phys.* **8** (1967), 2351–2356.

[10] S. L. Adler, and T. Piran, "Relaxation methods for gauge field equilibrium equations," *Rev. Mod. Phys.* **56** (1984), 1–40.

[11] M. T. Jones and P. E. Plassmann, "Scalable iterative solution of sparse linear systems," preprint MCS-P277-1191, Mathematics and Computer Science Division Division, Argonne National Laboratory (1991).

[12] M. K. Kwong, "Sweeping algortithms for inverting the discrete Ginzburg-Landau operator," preprint MCS-P307-0492, Mathematics and Computer Science Division Division, Argonne National Laboratory (1992). *Applied Mathematics and Computation*, to appear.

[13] K. J. M. Moriarty, E. Myers, and C. Rebbi, "A vector code for the numerical simulation of cosmic strings and flux vortices in superconductors on the ETA-10," *Computer Phys. Communications* **54** (1989), 273–294.

[14] M. M. Doria, J. E. Gubernatis. and D. Rainer, "Virial theorem for Ginzburg-Landau theories with potential applications to numerical studies of type-II superconductors," *Phys. Rev. B* **39** (1989), 9573–9575.